Climate Dynamics (2019) 52:5641–5656
https://doi.org/10.1007/s00382-018-4469-8

Climate warming will not decrease perceived low-temperature extremes in China

Jinxin Zhu[1] · Gordon Huang[4] · Brian Baetz[2] · Xiuquan Wang[3] · Guanhui Cheng[4]

Received: 29 November 2017 / Accepted: 23 September 2018 / Published online: 29 September 2018

Abstract
Temperature-related health metrics are often determined not only by temperatures but also by multiple climate variables. Temperatures compounded by other climate variables are of significant concern in the assessment of climate change impacts on public health. Temperatures, wind speeds and their combined effects are investigated here for a comprehensive study of how measured temperatures, perceived temperature, and their related extremes will change in China under climate change conditions. Future projections of combined temperatures and wind speeds over China are generated through the PRECIS regional climate modeling system. Results indicate that temperatures can increase nearly 6 °C over China by the end of the twenty-first century from the baseline period (1976–2005) without considering the wind speed changes. However, by considering the combined effect of temperature and wind speed, the perceived temperatures over China are projected to decrease by 4.8 °C relative to the observed values in the baseline period. This unexpected drop in the future perceived temperatures suggests the projected warming is likely to be offset to a large extent by a potential increase in wind speed. This may be related to the RCM's high-resolution making the thermal contrast distribute at finer scales. The mechanism behind this result needs to be further investigated to help understand the related physical processes and the associated uncertainties at regional scales. As for low-temperature extremes, China is projected to experience an apparent decrease in the frequency and duration of extreme cold events in the future compared to the baseline period without considering the combined wind chill effect. Considering the wind chill effect, an opposite trend for extreme cold events is detected, with an increase by 21% in the frequency of temperatures below − 20 °C.

Keywords Temperature and extremes · Wind chill · Dynamical downscaling · China · RCPs.

1 Introduction

Temperature as one of the most important climate variables has a significant impact on fatalities from weather-induced disasters in China (Zhai and Pan 2003; Wang et al. 2015c; Lin et al. 2016; Ma et al. 2017). Low-temperature extremes account for more deaths than high-temperature extremes do every year in China (Chen et al. 2013; Fang et al. 2015). Moreover, the low-temperature can be combined by wind speed to bring surplus cold stress to human body (Brown 2015). Human body loses heat mainly through the convection way. The convection from a warm surface heats the air around it to form an insulating boundary layer of warm air against the low-temperature. Wind disrupts this boundary layer and accelerates the evaporation process, therefore increasing the latent heat loss. To measure the combined effects on human thermal comfort, wind chill temperature is introduced to account for the perceived low-temperature.

Electronic supplementary material The online version of this article (https://doi.org/10.1007/s00382-018-4469-8) contains supplementary material, which is available to authorized users.

✉ Gordon Huang
huang@iseis.org

1 Department of Land Surveying and Geo-Informatics, Hong Kong Polytechnic University, Hong Kong, China

2 Department of Civil Engineering, McMaster University, Hamilton, ON L8S 4L7, Canada

3 School of Climate Change and Adaptation, University of Prince Edward Island, Charlottetown, PE C1A 4P3, Canada

4 Institute for Energy, Environment and Sustainability Communities, University of Regina, Regina, SK S4S 0A2, Canada

The combined effect results in increasing the risk of adverse health effects such as frostbite and hypothermia in some extreme conditions. To this end, low temperatures and wind are considered as well-established risk factors for human health. For a comprehensive assessment of the combined effects of these two risk factors under climate change, it is imperative to take into account the uncertainties in both contributing variables. Despite the knowledge about the combined effect of temperature and wind, it is often ignored in the context of climate projections. For example, the Fifth Assessment Report of the Intergovernmental Panel on Climate Change provides projections of many variables including temperature and wind, but the wind chill temperature is not analyzed nor discussed within the report (Hartmann et al. 2013).

Some recent studies have quantified how low-temperature extremes will change in China in the future. Yao et al. used simulations from eight General Circulation Models (GCMs) of the new Climate Model Intercomparison Project phase 5 (CMIP5) to investigate temperature extremes in China. As projected by multi-model ensembles under the RCP4.5 scenario, low-temperature extremes in China will decrease in the future, with the greatest change taking place in the early twenty-first century (Yao et al. 2012). Xu et al. studied changes in climate extremes in China in the twenty-first century through a high-resolution Regional Climate Model (RCM). They concluded that there would be a substantial warming in annual mean temperature and a significant decrease in low-temperature extremes in the future (Xu et al. 2013). As low-temperature extremes are projected to decrease by GCMs and RCMs, relatively few studies have been carried out to investigate how the wind speed over China will respond to climate change. Jiang et al. projected the wind speed across China with a significant declining trend by using three GCMs and RCMs under SRES A1B (Special Report on Emissions Scenarios) (Jiang et al. 2010, 2013). Although there are declining trends in both low-temperature extremes and wind speeds, it can not be simply concluded that the wind chill temperature will be less of a concern under climate change conditions. The uncertainty in the wind chill temperature is not the combination of the uncertainties for the two independent variables. It is the joint behavior of uncertainties in low-temperatures and wind speed that is of interest. However, there have been no previous studies that address the joint uncertainty of low-temperatures and wind speed as well as their combined effect.

The objective of this study is to analyze how the wind speed will change the temporal and spatial distributions of low-temperature and its corresponding extremes in response to climate change. Combined low-temperature extremes and wind speeds will be projected through an RCM. The selected RCM's skill in reproducing the historical climate over China will be gauged through validating its historical simulation with a dataset in terms of observed temperatures and wind speeds. After the validation, the independent climate variables will be projected from a dynamical downscaling under different greenhouse gas emission scenarios. Projections will be combined to quantify the impacts of wind speed on low-temperature extremes. The impacts of climate change on temperature extremes and wind speeds can then be assessed comprehensively by considering the joint behavior of the respective variable uncertainties.

2 Models, experimental design and data

The RCM used in this study is the Providing REgional Climate Impacts for Studies (PRECIS) model (Jones et al. 2004; Wilson et al. 2015). PRECIS is an atmospheric and land surface model which is designed with high resolutions for operational forecast and satisfying atmospheric research needs. The model has been widely applied to produce the high-resolution historical simulations and future projections (Xu et al. 2006; Feng et al. 2012; Wang et al. 2014, 2015D), and exhibits improvements in its simulation compared to its driving GCM (Wang et al. 2015c). The model's driving GCM is the Hadley Centre Global Environment Model version 2—Earth Systems (HadGEM2-ES) which is developed by the Met Office Hadley Centre for the CMIP5 (Collins et al. 2008). In the CMIP5, there are over 40 GCMs participating in the project. But only eleven out of these GCMs have been added to its capability to explicitly represent biogeochemical processes which can interact with the physical climate (MACA 2017). The HadGEM2-ES is not only included but also has the highest resolution of these eleven models (Martin et al. 2011; Jiang et al. 2015). Studies indicate that higher horizontal resolution is associated with the enhanced skill in representing climatic variables in the CMIP5 models (Colette et al. 2012; Rupp et al. 2013; Zhang et al. 2013). Plus, the ability of HadGEM2-ES to represent well most variables especially surface conditions and atmospheric circulation has been verified in these studies. Overall, the HadGEM2-ES exhibits relatively high skills in providing the Lateral Boundary Conditions for driving the PRECIS model over China.

The computational domain of the PRECIS simulation covered China with a $0.44° \times 0.44°$ spatial resolution. Considering the geographical features of temperature changes in China and based on some previous studies (Li et al. 2011; Luo et al. 2013; Bucchignani et al. 2014), the contiguous China domain were divided into five sub-regions, namely Northwest China, Northcentral China, Tibet, Northeast China, and South China. As shown in Fig. 1, these sub-regions are typically used in weather and climate-related research in China because of the climatic

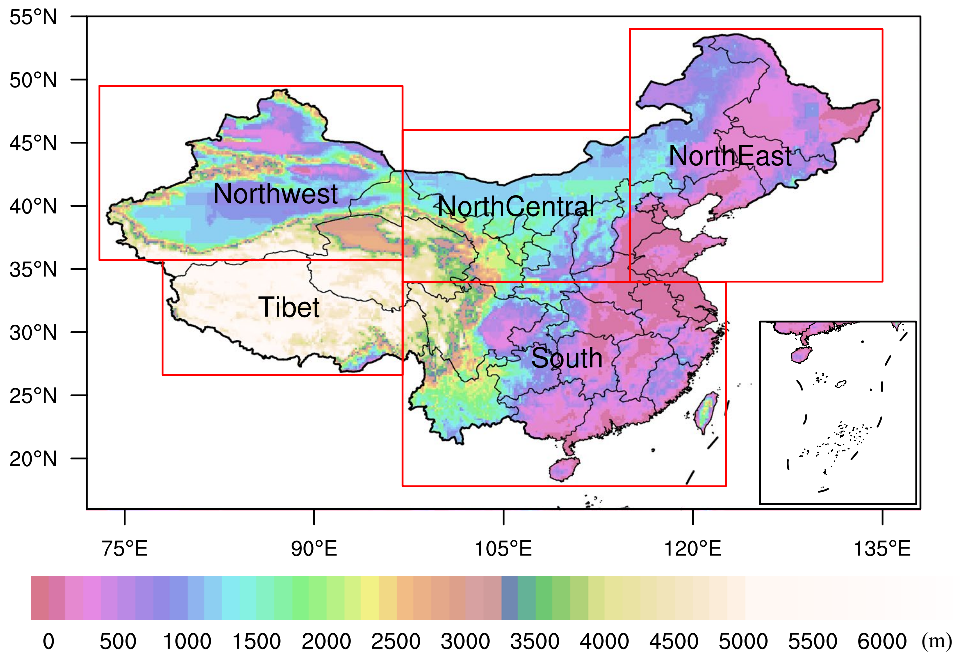

Fig. 1 Model domain, topography (unit: m), and the five sub-regions: Northwest, North-central, Northeast, Tibet, and South China

similarities within each sub-region. The temperature indices for representing extreme events can be divided into two main categories, namely high-temperature indices and low-temperature indices. As the objective of this study is to investigate the combined effects of temperature and wind speed. The combined effects are effective when low-temperature is compounded by wind speed. Therefore, five low-temperature indices were selected in this study and are described in detail in Table 1 (Frich et al. 2002). The PRECIS model ran continuously from1969 to 2005 for the historical simulation and from 2006 to 2099 for the future projections. To assess the skill of the model in simulating the historical climate, model results were validated with an observation dataset and a reanalysis dataset for the baseline period from 1976 to 2005. The Climate Research Unit (CRU) monthly gridded dataset was selected as the observation dataset with a spatial resolution of 0.5° × 0.5° for the mean, maximum and minimum temperatures. The CRU dataset applies enhancement with a quality control algorithm to develop the global climate variables with a high-resolution in time and space (Harris et al. 2014). However, the variables in the CRU dataset do not include the wind speed. An ERA-Interim reanalysis dataset, therefore, was adopted in this study to validate the dynamical downscaled wind speed in terms of spatial and temporal patterns. Future simulations were forced with specified concentrations consistent with a medium emission scenario (RCP4.5) and a high emission scenario (RCP8.5) (Moss et al. 2010; Van Vuuren et al. 2011). With these two scenarios, changes in temperature, wind speed, and their combined effect subject to increasing radiative forcing were investigated.

Table 1 Definitions of extreme temperature indices used in this study

Labels	Name	Index definition	Units
FD	Frost days per period	The counted number of days where the daily minimum temperature is less than 0 °C	1
ID	Ice days per period	The counted number of days where the daily maximum temperature is less than 0 °C	1
TN10p	Percentage of days when TN < 10th percentile	The percentage of time where the daily minimum temperature is less than the 10th percentile of daily minimum temperature for the reference period	%
TX10p	Percentage of days when TX < 10th percentile	The percentage of time where the daily maximum temperature is less than the 10th percentile of daily maximum temperature for the reference period	%
CWFI	Cold spell days	Annual count of days with at least 6 consecutive days when the daily minimum temperature is less than the 10th percentile	1

3 Simulations of historical temperature and wind

Figure 2 shows the spatial patterns of annual mean, maximum and minimum temperatures distributed over China. The patterns were derived from HadGEM2-ES, PRECIS, and CRU for the period from 1976 to 2005. The patterns from the observation dataset show that all temperatures are relatively high over South China and relatively low over Tibet and Northeast China. Compared to CRU, HadGEM2-ES simulates a similar distribution but with a holistic overestimation of the magnitude of the annual mean temperature. As for the other two variables, the GCM overestimates the magnitude for the annual maximum temperature and underestimates the annual minimum temperature. It can be also found that the absolute magnitude overestimated for the annual maximum temperature outweighs the value underestimated for the annual minimum temperature. These non-uniformities between the observational and simulated temperatures are common occurrences not only in HadGEM2-ES but also in many other GCMs (Flato et al. 2013; Zhou et al. 2013). The occurrences are successfully eliminated by the PRECIS model through dynamical downscaling. The RCM significantly improves the accuracy of simulation and better depicts the geographical distribution of temperatures than its driving GCM over China. It captures the warm centers located in the Szechwan Basin (30°30′N, 105°30′E) and the Pearl River Basin (30°22′N, 89°44′W) in South China and the cold center at the Tibetan Plateau for all three temperatures.

To gauge the skills of HadGEM2-ES and PRECIS in reproducing the temporal patterns of annual mean, maximum

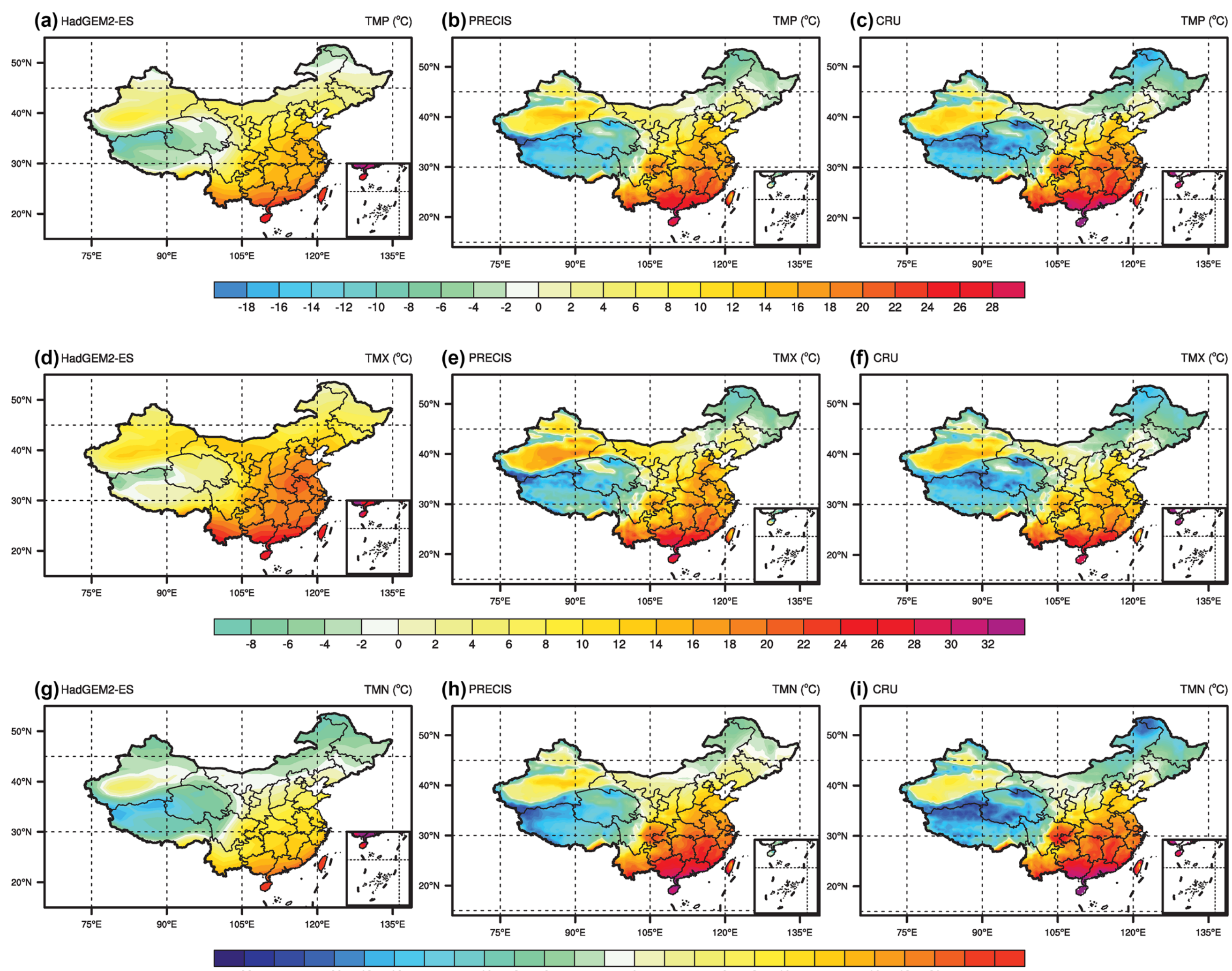

Fig. 2 Spatial distributions of mean (TMP), maximum (TMX) and minimum (TMN) temperatures (unit: °C) over China from HadGEM2-ES (**a, d**, and **g**), PRECIS (**b, e**, and **h**), and observations (CRU) (**c, f**, and **i**) for 1976–2005

and minimum temperatures, the annual cycle is introduced to summarize how closely the patterns from two models' results match the observations. As shown in Fig. 3, the relative merits of HadGEM2-ES and PRECIS are exhibited in reproducing the temporal curves of annual mean, maximum and minimum temperatures with respect to the statistical values of each month in the baseline period. The curve of HadGEM2-ES is holistically 1.7 °C above the observational curve for the annual mean temperature, 2.1 °C above for the annual maximum temperature, and 2.3 °C below for the annual minimum temperature. On the other hand, the curve of PRECIS matches well with the annual cycle of CRU for all temperatures. The PRECIS model only overestimates the temperatures in July by approximately 1.6 °C and slightly underestimates the temperatures in October and November. Other than these, the curve of PRECIS generally follows the curve of CRU. This indicates that PRECIS has a relatively high skill in reproducing the temporal distribution of temperatures over China. Overall, it is evident that PRECIS outperforms HadGEM2-ES, and PRECIS adds value to its driving GCM with respect to simulating the temporal and spatial patterns of annual mean, maximum and minimum temperatures for China.

To validate the skill of the PRECIS model in simulating the historical wind speed, monthly reanalysis data from the ERA-interim were used. As shown in Fig. 4, the reanalysis dataset shows that the annual mean wind speed is relatively high from east to west across Inner Mongolia (44°0′N, 113°0′E), the Tarim Basin (39°0′N, 83°0′E), and the Tibetan Plateau. The high wind speed area is between 30°N and 60°N where the prevailing westerlies are located. Studies indicate that the prevailing westerlies have direct impacts on driving the surface wind (Wang et al. 2015a). Comparing to the reanalysis data, HadGEM2-ES does capture the high wind speed across Inner Mongolia, but it underestimates the wind speed across the entire nation and simulates two artificial low wind speed centers in the Sichuan Basin (30°30′N, 105°30′E) and the Tarim Basin. The PRECIS model successfully eliminates these underestimations and reasonably reproduces the high wind belt across Inner Mongolia, the Tarim Basin, and the Tibetan Plateau. In addition, the PRECIS model simulates closer magnitudes of wind speed in China than its driving GCM. In Fig. 5, the annual cycles are used to compare the skills of HadGEM2-ES and PRECIS in reproducing the temporal patterns of wind speed. The curve representing the reanalysis dataset shows high values in March, April, and May the 3 months from the spring season in China when it is also the windiest period in a given year (Gong et al. 2011). During this period, there could be a rapid fall in temperature accompanied by strong winds. The

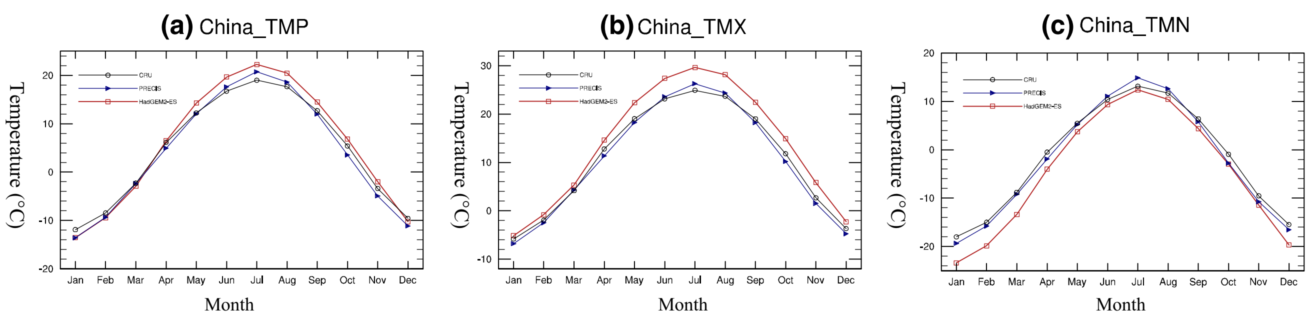

Fig. 3 Annual cycles of the mean (TMP), maximum (TMX) and minimum (TMN) temperatures (unit: °C) over China for 1976–2005

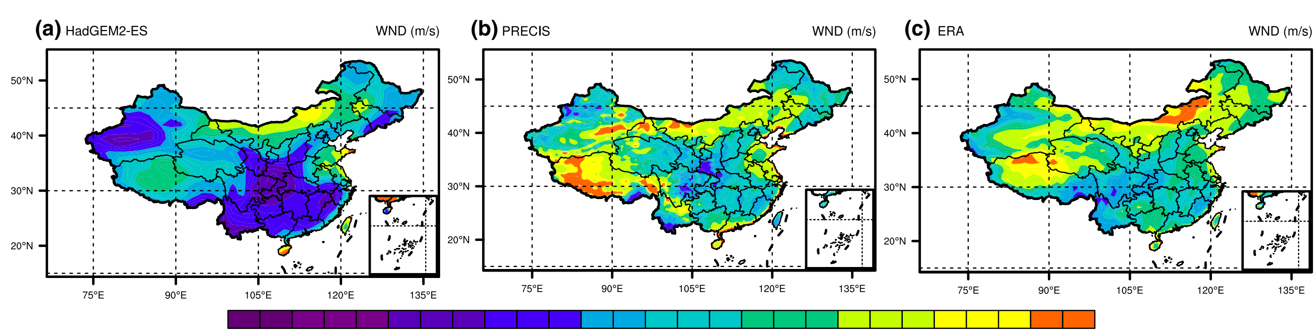

Fig. 4 Spatial distributions of mean wind speed (unit: m/s) over China from HadGEM2-ES (**a**), PRECIS (**b**), and Reanalysis (ERA) (**c**) for 1976–2005

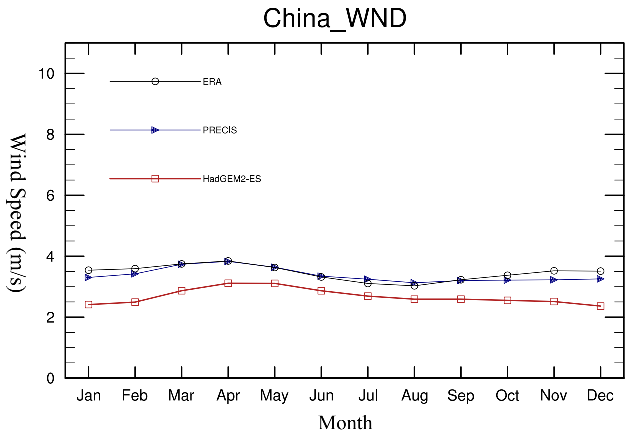

Fig. 5 Annual cycle of wind speed (unit: m/s) over China from HadGEM2-ES (**a**), PRECIS (**b**), and Reanalysis (ERA) (**c**) for 1976–2005

PRECIS model successfully captures the peak of the wind speed in the annual cycle. For the remaining three seasons, the annual cycle of the RCM matches well the cycle of the reanalysis dataset except for some slight underestimations. The entire curve of HadGEM2-ES is approximate by 0.6 m/s below the curve of the reanalysis dataset, thus failing to capture the peak value in Spring. Therefore, it is found that the PRECIS model, with its simulation of finer scale physical processes, can better depict the distributions of wind speed than its driving GCM for China. Overall, a high-resolution simulation is essential to obtain reliable temporal and spatial patterns of wind speed over China. In addition, the downscaling approach generally simulates more reliable spatial distributions of the mean temperature, maximum temperature, minimum temperature and wind speed than its driving GCM in China and five subregions with higher correlation coefficients and lower root mean square errors (Table 2). The simulated wind chill is also verified to the observed wind chill for the baseline period (refer to the supplementary material). PRECIS, with eliminations of overestimations in wind chill temperatures, has a relatively higher skill of reproducing the spatial distribution of wind chill temperature over China than HadGEM2-ES.

4 Projections of future temperature and wind speed

With the reasonable reproduction of historical climate, a premise is created for projecting a plausible range of future climatic conditions. The temperatures and wind speed are projected by the PRECIS model under RCP4.5 and RCP8.5 scenarios for the period from 2006 to 2100. To better understand the changes in the variables, the continuous simulation period was divided into two periods, namely the period 2036–2065 (the 2050s) and the period 2070–2099 (the 2080s). The changes in the annual mean, maximum, minimum temperatures and wind speed are calculated by subtracting the values in the baseline period from the values projected under two RCPs for the 2050s and the 2080s over China. The changes in the spatial patterns of temperatures are exhibited in Fig. 6 for both periods relative to the baseline period. It can be found that there are positive changes from 0.3 to 6 °C for all the maps. The positive changes are increasing from the 2050s to the 2080s in terms of all three temperatures. For each period, there is no large difference between the annual mean minimum temperature and the annual mean maximum temperature in terms of the warming magnitude. The warming magnitude in the northern subregions (Northwest China, Northcentral China, Northeast

Table 2 Statistical summary of correlation coefficient and root mean square errors for model simulations of four climatic variables in china and five subregions during 1976–2005

Regions	TMP		TMX		TMN		WND	
	RCM	GCM	RCM	GCM	RCM	GCM	RCM	GCM
Root mean square error								
China	1.835	2.698	1.832	3.341	2.056	2.557	0.608	0.924
NW	1.906	4.310	2.112	5.026	2.332	4.047	0.547	0.988
CN	0.898	1.944	1.238	2.207	1.274	2.164	0.617	0.745
NE	1.224	1.744	0.694	2.134	2.070	2.783	0.593	0.934
Tibet	1.965	3.710	1.889	5.126	2.531	3.169	0.833	0.943
SC	1.599	2.462	1.873	2.895	1.647	2.173	0.691	0.909
Correlation coefficient								
China	0.977	0.869	0.978	0.960	0.967	0.869	0.904	0.890
NW	0.938	0.652	0.941	0.650	0.911	0.633	0.687	0.671
CN	0.982	0.868	0.975	0.840	0.969	0.856	0.914	0.853
NE	0.988	0.935	0.987	0.942	0.955	0.914	0.840	0.836
Tibet	0.978	0.885	0.974	0.863	0.969	0.887	0.822	0.385
SC	0.984	0.941	0.976	0.918	0.984	0.949	0.881	0.792

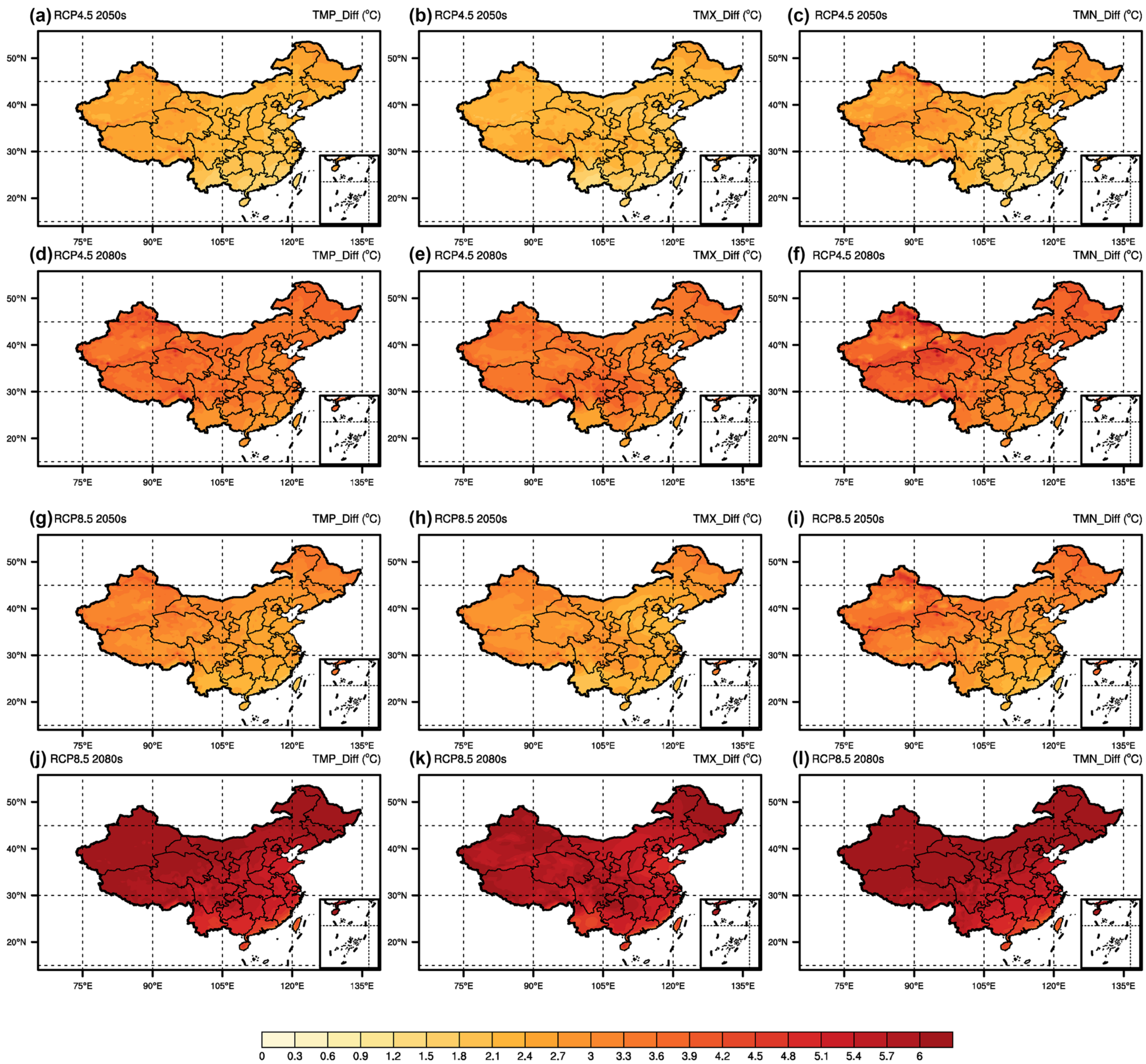

Fig. 6 Spatial distributions of changes in the mean (TMP_Diff), maximum (TMX_Diff) and minimum (TMN_Diff) temperatures (unit: °C) as projected by PRECIS for two future periods (2036–2065 relative to 1976–2005 and 2070–2099 relative to 1976–2005)

China, and Tibet) is slightly larger than the southern sub-region (South China). The main reason why the northern sub-regions except Tibet have higher warming rates than the southern sub-region is that their relatively high latitudes make them receive more positive albedo-temperature feedback. As for Tibet, its high-elevation increases the melting process of the ice and snow cover under a warming climate. The melted ice and snow increases water vapor which traps more heat at the surface and makes the surface less reflective and adds to the warming effect (Wang et al. 2015b). But the warming effect is shown to shrink to smaller areas for the maximum temperature than for the minimum temperature.

In terms of comparison between warmings under different scenarios, the RCM projects a larger warming degree under RCP 8.5 than under RCP4.5 for each period. Especially in the 2080s, the contrast becomes more significant with an increase in the radiative forcing. The results derived from the PRECIS model are congruent with the results of Yu's research through WRF driven by CAM and Gao's research through RegCM driven by BCC-CSM1.1 over China (Yu et al. 2010; Gao et al. 2013).

For the temporal patterns, Fig. 7 demonstrates the changes in the annual cycles in terms of three temperatures for China under two RCPs for both future periods. All three charts

Fig. 7 Future changes in annual cycles of the mean (TMP), maximum (TMX) and minimum (TMN) temperatures (unit: °C) over China for two future periods

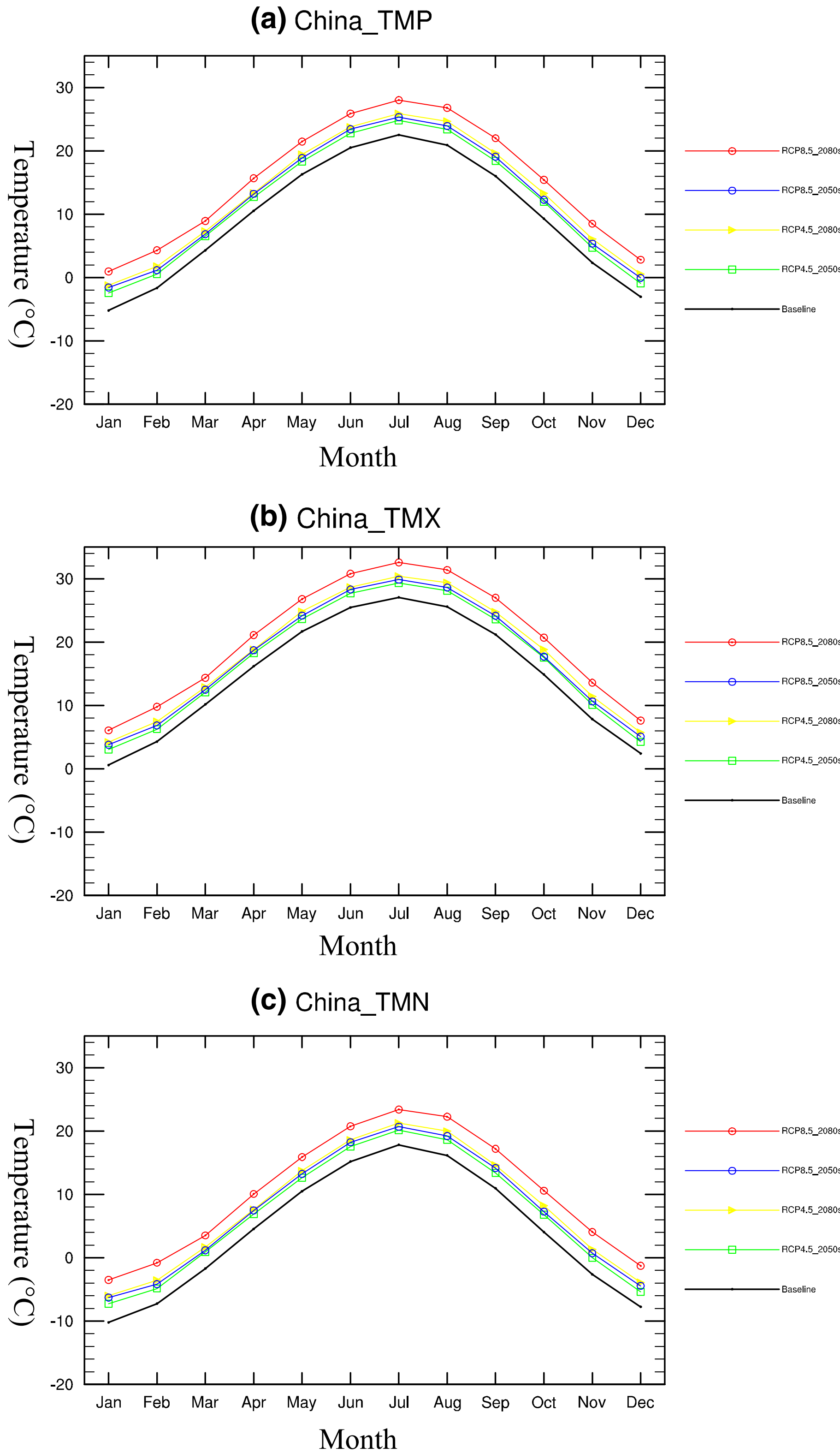

show that four curves for the future are above the curve for the reference period which means temperatures over China have positive changes under each scenario for 12 months. It is also apparent that the future warming magnitudes relative to the baseline period are approximately the same for all three temperatures. This warming trend is consistent with the results obtained from Fig. 7 where there was also no large difference among the three temperatures in terms of the warming magnitude. Therefore, it can be concluded that the greenhouse effect would be equally effective for impeding radiative forcing from escaping into space during the day-time (represented by the maximum temperatures) and night-time (represented by the minimum temperatures). The increments in temperature are positively correlated with an increase in the radiative forcing. In detail, these increments can be separated into two categories, a 5.4 °C increment for the curve under RCP8.5 for the 2080s and a 2.6 °C increment for the other three curves (RCP4.5 for the 2050s, RCP4.5 for the 2080s, and RCP8.5 for the 2050s) with respect to every temperature index. The three curves generally coalesce together because their radiative forcing levels are all at the medium level. When the radiative forcing level reaches the maximum, the increments in the temperatures are more than double of those under the medium emission scenario. Thus, the warming trend can be amplified with an increase in the radiative forcing.

The projected changes in the wind speed relative to the baseline period under two RCPs for two periods are displayed in Fig. 8. The PRECIS model projects a nearly 30% increase in the wind speed over China for all four maps except – 10% to – 5% decreases in some parts of Tibet under RCP8.5 for the 2080s. This result is opposite to the findings from the results from the IPCC reports (Sperber et al. 2013; Song and Zhou 2014; Sun et al. 2015). Since these reports are based on the results from GCMs, the projections of wind speed under RCPs from the driving GCM, HadGEM2-ES are examined. The GCM does project up to a 15% increase over most parts in South China and the Amur Basin (52°56′N, 141°5′E) in Northeast China under both RCPs for two future periods. However, there are nearly 21% decreases projected by the GCM across Inner Mongolia, the Tarim Basin, and the Tibetan Plateau which historically are the high-wind regions. The GCM tends to enhance the decreasing trend over these areas with radiative forcing increasing. As for the areas with increasing wind speed marked as yellow in the maps, they will also expect a diminished tendency from medium to high emissions scenario. This may be related to the enhanced warming under climate change which reduces the thermal contrast between low latitude and high latitude areas (Christensen et al. 2007; Hewitson et al. 2014). The PRECIS model simulates a decreasing trend in the wind speed over China with increases in radiative forcing for both future periods. But the trend is not as detectable as the trend simulated by its driving GCM. Despite the trend, the PRECIS model projects stable positive changes in the wind speed over China which is contrary to the simulations from its driving GCM that show decreases across three historically high-wind regions. This may be related to that RCM's high-resolution make the thermal contrast distribute at finer scales. Plus, it has been found that the driving GCM tends to underestimate the wind speed over China through the model validation. But the mechanism behind this result from the RCM needs to be further investigated in terms of related physical processes and the associated uncertainties at regional scales.

Figure 9 demonstrates the temporal changes relative to the baseline period in the annual cycles of wind speed for China. The black curve represents the values in the baseline period, the other four curves represent annual cycles under two RCPs for two future periods. The four curves are distributed in a distinct graduation from high to low wind speeds, namely the one under RCP 4.5 for the 2080s, the one under RCP 4.5 for the 2050s, the one under RCP8.5 for the 2050s, and the one under RCP8.5 for the 2080s. Under RCP8.5, the wind speed decreases slightly from the 2050s to the 2080s as the radiative forcing increases. Under RCP4.5,

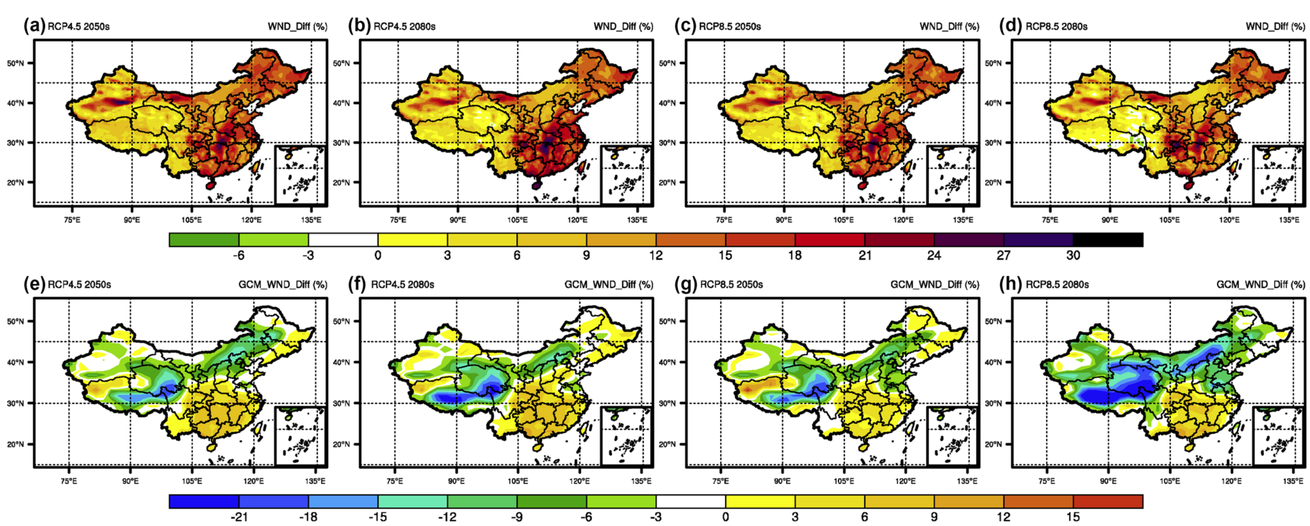

Fig. 8 Spatial distributions of changes wind speed (WND_Diff) temperature (unit: %) as projected by PRECIS for two future periods

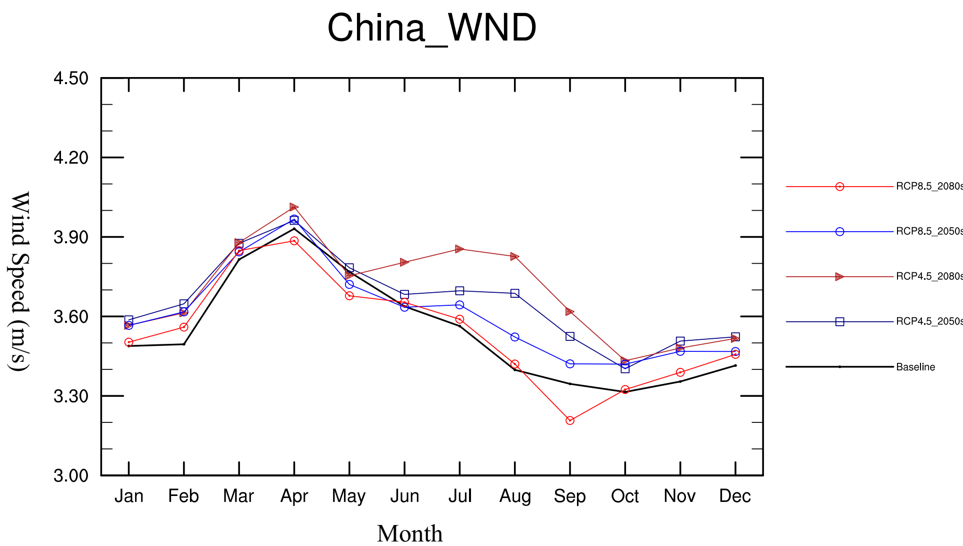

Fig. 9 Future changes in the annual cycle of wind speed (unit: m/s) over China for two future periods

the wind speed, however, increases slightly from the 2050s to the 2080s with stable radiative forcing. It is possible that the result is caused by natural variability or the uncertainty in the model (Wang and Huang 2015; Wang et al. 2015b, 2018). Compared to the black curve, there are three curves (under RCP 4.5 for the 2080s, under RCP 4.5 for the 2050s, and under RCP8.5 for the 2050s) above it and one curve (under RCP8.5 for the 2080s) slightly below it. The values below the baseline results cab be explained by the diminished thermal contrast caused by the enhanced warming under the high radiative forcing scenario. The three curves above the black one generally stick together as their radiative forcing is relatively at the same level. This is constant in the annual cycles for the three temperature conditions. The most distinct difference between three curves and the black one is that their projected values have significant increments relative to the baseline for the Summer and Autumn months. As for the Spring and Winter months, there are only indiscernible increases from the black curve. These results illustrate that the wind speed will increase and then maintain the level or slightly decrease with the radiative forcing increasing.

To investigate how the combined effects of temperature and wind speed will change under climate change, the wind chill temperature was studied as it is defined as the perceived temperature decrease due to the air flow. The wind chill temperature (*wct*) was computed from the wind speed (v) and surface air temperature (T) by the conversion equation from Environment and Climate Change Canada (Environment Canada 2014). This approximation requires the surface air temperature to be in a validation range between − 50 and 5 °C and the wind speed at 10 m above the surface. After checking the output data from the RCM, no temperature was found below − 50 °C. For temperatures above 5 °C, the equation would not be applied.

$$wct = 13.12 + 0.6215T - 11.37(3.6v)^{0.16} + 0.3965T(3.6v)^{0.16}$$

The equation was applied to the daily temperatures and wind speed in the baseline period and the continuous simulation period from 2006 to 2100. To calculate the differences in the wind chill temperature between the future and the present, the wind chill temperatures in the baseline period are subtracted from the wind chill temperatures under two RCPs for the 2050s and the 2080s. Figure 10 shows the changes in the calculated wind chill temperatures in terms of annual mean, maximum and minimum temperatures under both RCPs for two future periods. Contrary to what was anticipated, the RCM projects decreases over the entire nation under RCP4.5 for the 2050s, under RCP4.5 for the 2080s, and under RCP8.5 for the 2050s. Particularly, the maximum decrease (− 4.8 °C) is projected to take place over the Tibetan Plateau and Inner Mongolia. Moreover, these two regions are projected to have the maximum negative change and form two cooling centers for the perceived temperature throughout the entire period. Other than the two centers, the other areas in China will only have some increases in the perceived temperatures under RCP8.5 for the 2080s. Therefore, the perceived temperatures are projected to be lower over China in the future than in the reference period. The reason for this unexpected drop in temperatures is that the PRECIS model projects great warming accompanied with increases in the wind speed. Particularly, the wind speed increases significantly in Autumn, and this season will expect the most frequent cold waves taking place in the future. The mechanism that the model projects great warming with a correlated strong increase in the wind speed will be further investigated in future research.

The relationships between changes in the mean temperature and the corresponding changes in the extreme temperature events are nonlinear. Small changes in the mean temperature sometimes can result in relatively large changes in the probabilities of these extreme events

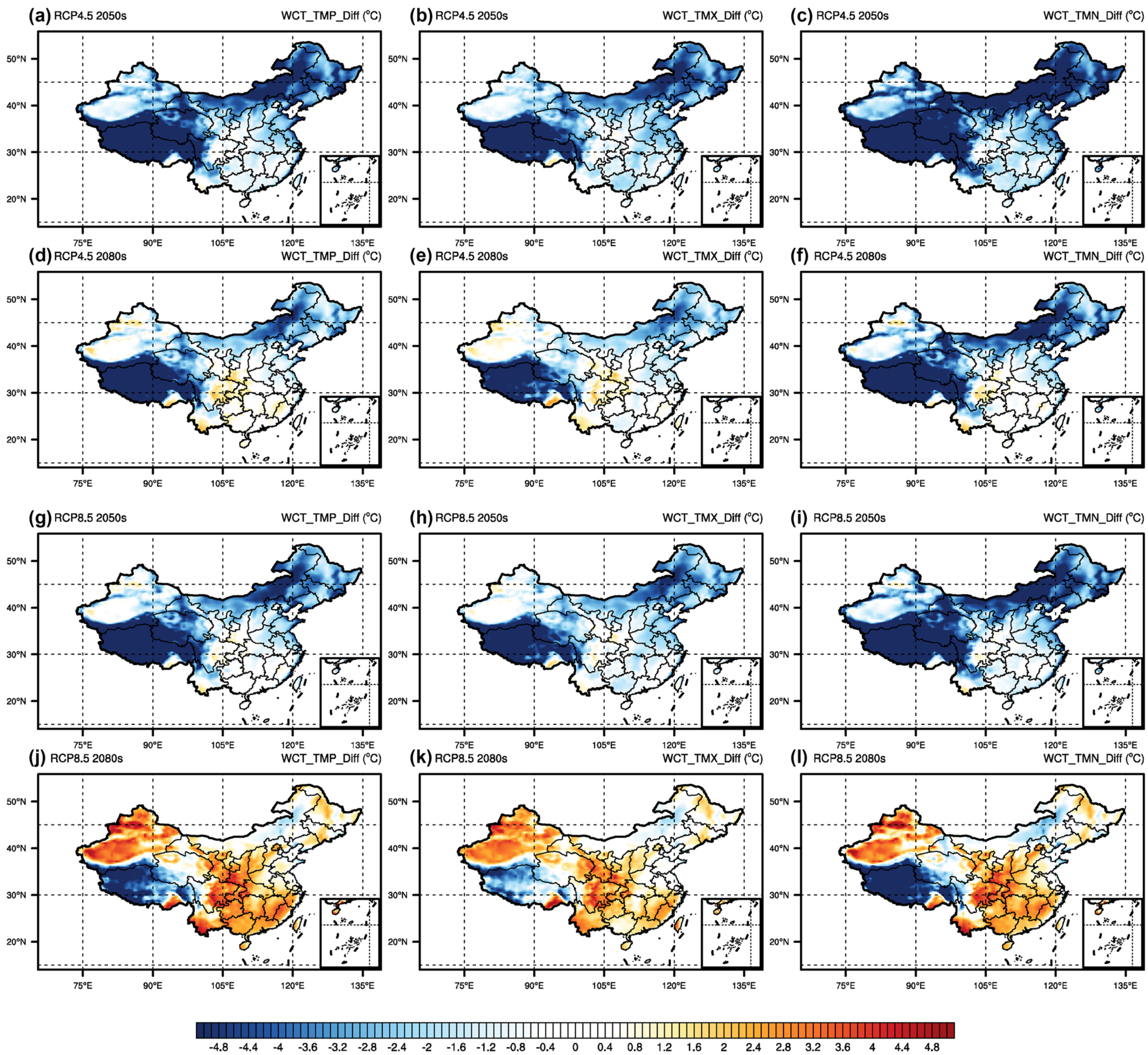

Fig. 10 Spatial distributions of changes in wind chill mean (WCT_TMP_Diff), maximum (WCT_TMX_Diff) and minimum (WCT_TMN_Diff) temperatures (unit: °C) as projected by PRECIS for two future periods

(Mearns et al. 1984). First, the projected changes relative to the reference period in the five selected indices of low-temperature extremes in China under RCP4.5 and RCP8.5 are investigated for two future periods (as shown in Fig. 11). The indices of low-temperature extremes can be divided into three categories, namely threshold indices (FD and ID), percentile indices (TN10p and TX10p) and duration index (CWFI). Results for both FD and ID have negative changes across the nation, and the maximum decrease takes place in South China and the minimum in Tibet. This means that China is likely to experience a lower number of FD and ID under RCPs in the future. Changes in both indices under RCP4.5 are relatively consistent with the changes under RCP8.5 for two future periods. The two threshold indices are insensitive to the mean temperatures arising from an increase in the radiative forcing. As for the two percentile indices, they are relatively more sensitive to the mean temperature changes induced by climate change. Given a future period, the nation will have a lower percentage of extremely cold days with the radiative forcing increases from RCP4.5 to RCP8.5. Relative to the baseline period, the percentage of extreme events drops from 10% which means China is likely to experience a lower frequency of extremely cold days in the

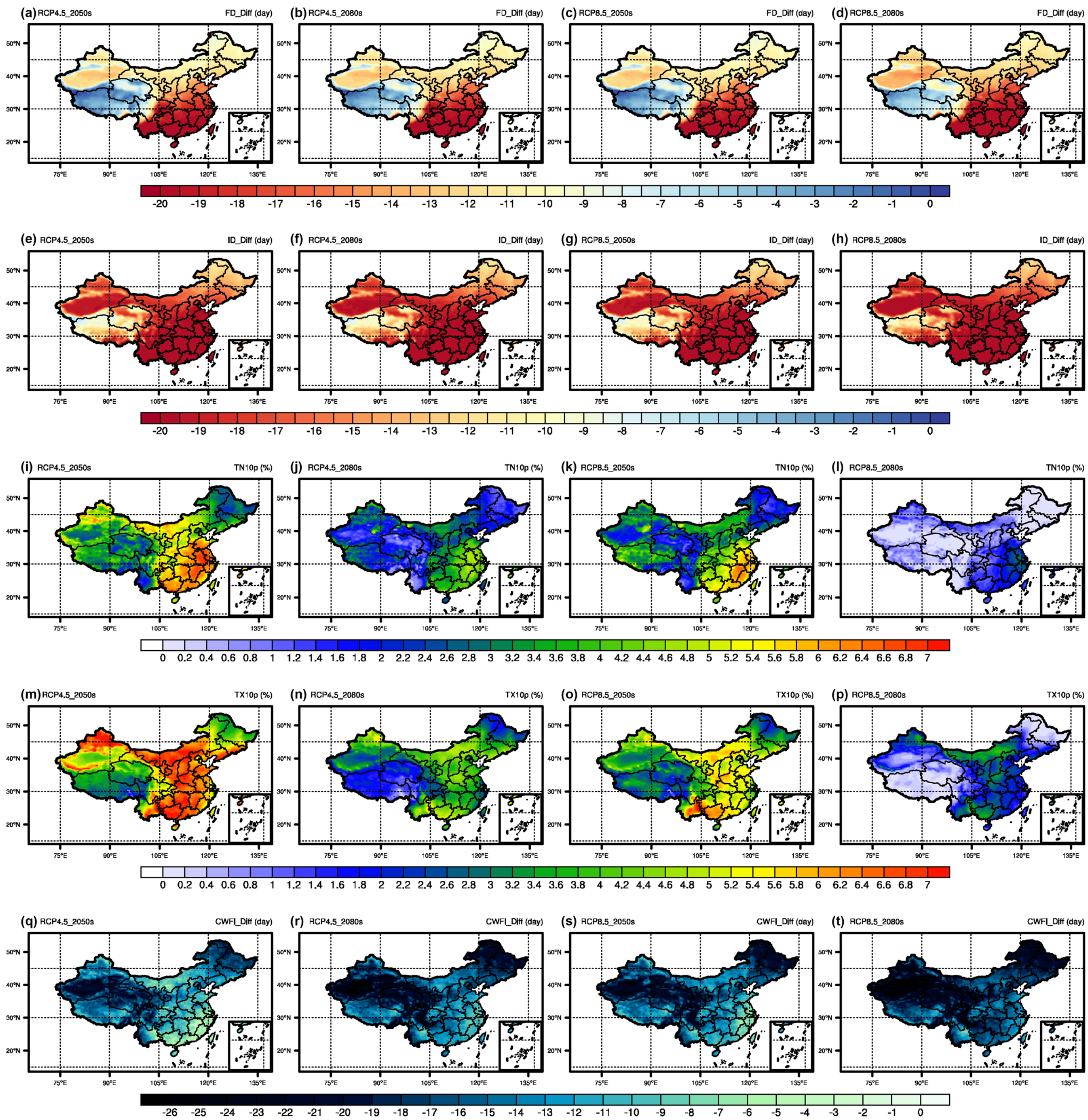

Fig. 11 Spatial distributions of projected indices of low-temperature extremes (FD, unit: day; ID, unit: day; TN10p, unit: %; TX10p, unit: %; CWFI, unit: day) in China under RCP4.5 and RCP8.5 for two future periods

future. Both percentile indices have the maximum change over Tibet and the minimum change over South China and Northcentral China throughout the entire period. Although the patterns of TN10p are consistent with those of TX10p concerning geographical differences, the magnitude of change in TX10p is greater than that in TN10p. Interestingly, the magnitude of change in the minimum temperature where TN10p is derived is larger than that in the maximum temperature where TX10p is calculated. This opposite trend further proves that the relationships between changes in the mean temperature and changes in the probability of corresponding extremes are nonlinear. Lastly, the geographical patterns of changes in the duration index have negative changes in China under any RCP for any period. These decreases in the CWFI are amplified by an increase in radiative forcing. It is noted that the duration of extremely cold days will become shorter than before. Regionally, the maximum decrease of CWFI is across the Tarim Basin, the Qaidam Basin (37°16′N, 94°27′E), Hexi Corridor (36°2′N, 103°48′E) and the Amur Basin for all four maps. It can be concluded that China will experience an apparent decrease in the frequency and duration of extreme cold events in the future compared to the baseline period without considering the combined wind chill effect.

How will the probability of low-temperature extremes change in response to climate change with consideration of the wind chill effect? To investigate the changes in the probability of the low-temperature extremes compounded by wind speed and compare these to changes in the probability of extremes without combining the wind chill effect, histograms of the frequency distribution of the daily temperatures are introduced in this study. For each chart in Fig. 12, the daily temperatures of every grid cell in China are taken into account for the analysis. Each column represents the percentage of days that temperatures of all grids fall into a range (−70 to −60 °C, −60 to −50 °C, −50 to −40 °C, −40 to −30 °C, −30 to −20 °C, −20 to −10 °C, −10 to 0 °C) in the baseline period, and each dot from the lines represents the percentage under an RCP scenario for a future period. As this study focuses on low-temperature extremes, only temperatures below 0 °C are analyzed. The minimum value in the analyzed temperatures is −68 °C, therefore, a −70 °C threshold was chosen as the lowest boundary for the histogram. Results show that the RCM simulated the historical temperatures with no values below −40 °C, only less than 5.2% for the interval (−40 °C, −30 °C), and 94.8% for values above −30 °C. Without considering the effects of wind, the RCM projects decreases in the frequency of cold extremes and increases in the lowest temperature from −40 to −30 °C. Considering the combined effect of low-temperature and wind, the results show a totally opposite trend to the previous projections. There are increases in the frequency of extreme events and an apparent decrease in the lowest temperature. The percentage of lowest temperature, the interval (−70 °C, −60 °C), increases from 0 to 0.2%. Comparing the probabilities of wind chill extremes to the regular ones, the wind speed mainly increases up to 21% in the frequencies of low-temperatures below −20 °C. For these temperatures, the daily maximum temperatures are more sensitive to the wind chill effect than the minimum temperatures. The magnitude of increase calculated for each interval for the maximum temperatures is larger than that for the minimum temperatures. Compared to the wind chill effect, temperatures are much less sensitive to changes in the radiative forcing. The increase in the radiative forcing slightly strengthens the negative changes in the frequency of cold extremes and lifts the lowest temperature to some extent. For instance, the curves under RCP8.5 become somewhat steeper than the curves under RCP4.5 for the 2080s when there is a significant difference between the radiative forcing levels.

5 Conclusions

In this study, the PRECIS model is employed to investigate low-temperature extremes and wind speed in response to climate change at a national level with consideration of the combined effect among climate variables. Changes in temperature extremes, wind speed and wind chill temperatures for China under two RCPs were investigated for two future periods. The RCM's skill in simulating the climate over China for the historical period was gauged and a reasonable reproduction of historical temperatures and wind speeds was obtained through validation with the observation and the reanalysis datasets in terms of spatial and temporal patterns. After the validation, a plausible range of future temperatures and wind speeds were projected under RCPs to further investigate how the joint projections of low-temperatures and wind speed will change in response to global warming.

It was found that all changes in temperatures relative to the baseline period are positive in the spatial and temporal patterns of temperatures under two RCPs for both future periods. In terms of comparison between warmings under different scenarios, the RCM projects a larger warming degree under RCP 8.5 than under RCP4.5 for each period which means the increments in the temperatures are positively correlated with an increase in the radiative forcing. When the radiative forcing level reaches the maximum, the increments in the temperatures are more than the double of those under the medium emission scenario. Opposite to what has been generally anticipated, PRECIS projects increases up to 30% in the wind speed over China for all four maps except −10 to −5% decreases in parts of Tibet under RCP8.5 for the 2080s. The patterns of wind speed simulated by the PRECIS model were found to be contrary to the simulation of its driving GCM regarding the decreases across three historical high-wind regions, Inner Mongolia, the Tarim Basin, and the Tibetan Plateau. This may be related to the RCM's high-resolution making the thermal contrast distribute at finer scales. Moreover, its driving GCM tends to underestimate the wind speed over China throughout the entire period. However, the mechanism behind this result still needs to be further investigated concerning the related physical processes and associated uncertainties at finer scale. The wind chill temperature is chosen to demonstrate how the combined effects of temperatures and wind speed will change over China under RCPs. Unexpectedly, the perceived temperatures are projected to decrease by −4.8 °C relative to the values in the baseline period over the entire nation. The reason for this unexpected drop in the perceived temperatures is that

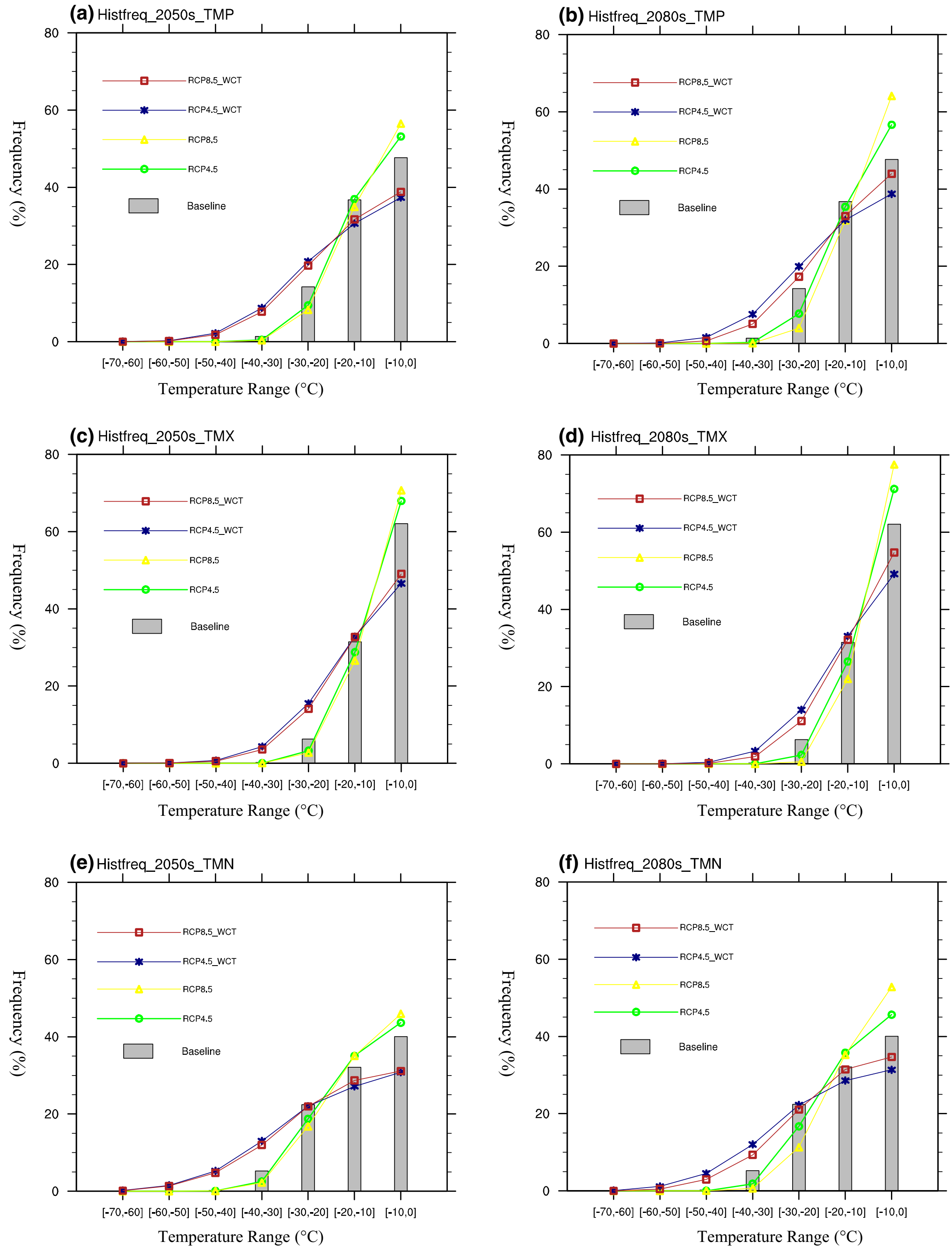

Fig. 12 Statistical changes in the frequencies of future low-temperature extremes (unit: %) relative to the reference period (1976–2005) with and without considering the wind chill effect in terms of mean (TMP), maximum (TMX) and minimum (TMN) temperatures

the PRECIS model projects great warming accompanied with increases in wind speed. The maximum decreases are projected to take place over the Tibetan Plateau and Inner Mongolia. Moreover, these two regions form two cooling centers which have the maximum negative changes for the perceived temperatures throughout the entire period. Other than these two centers, the rest of the areas in China are expected to have some increases in the perceived temperatures under RCP8.5 by the end of twenty-first century.

Without considering the wind chill effect, China can expect a lower number, less frequent and shorter duration extreme cold events under RCPs in the future than in the baseline period. In detail, the RCM projects all negative changes in FD and ID. These two threshold indices are insensitive to the mean temperatures arising from an increase in the radiative forcing. As for the two percentile indices, they are relatively more sensitive to the changes in mean temperatures induced by climate change. Relative to the baseline period, the percentile of extremes event drops from 10% which means China is likely to experience a lower frequency of extremely cold days in the future. Moreover, the magnitude of changes in TX10p is more significant than that in TN10p. Interestingly, the magnitude of changes in the minimum temperature where TN10p is derived is larger than that in the maximum temperature where TX10p is calculated. Lastly, the changes in the duration index are all negative regarding geographical patterns under any RCP for any period. It is noted that the duration of extremely cold days in China will become shorter than before. Through an analysis of three different types of cold extreme indices, it was concluded that the relationships between changes in the mean temperature and the corresponding changes in the extreme temperature events are nonlinear. Small changes in the mean temperature can sometimes result in relatively large changes in the probabilities of these extreme events. Considering the combined effects of low-temperature and wind speed, the results for extreme cold events show an opposite trend to previous projections. There are increases in the frequency of extreme events and decreases in the lowest temperatures. Comparing the probabilities of wind chill extremes to regular events, the wind speed is likely to result in a 21% increase in the frequencies of low-temperatures below − 20 °C. For these temperatures, the daily maximum temperatures are more sensitive to the wind chill effect than the minimum temperatures, since the increments relative to the reference period calculated from each interval for the maximum temperatures are more significant than those for the minimum temperatures.

Acknowledgements This research was supported by the National Natural Sciences Foundation of China (51809223), the Hong Kong Polytechnic University Start-up Grant (1-ZE8S), the China Scholarship Council, the Program for Innovative Research Team in University (IRT1127), the 111 Project (B14008), and the Natural Science and Engineering Research Council of Canada. Readers can find the data that support or underlie the conclusions presented in Climate Change Data Portal for China (http://chinaccdp.org/).

References

Brown A (2015) Climate science: North American cold spells. Nat Clim Change 5:515. https://doi.org/10.1038/nclimate2674

Bucchignani E, Montesarchio M, Cattaneo L, Manzi MP, Mercogliano P (2014) Regional climate modeling over China with COSMO-CLM: performance assessment and climate projections, J Geophys Res Atmos 119:12–151. https://doi.org/10.1002/2014JD022219

Chen R, Wang C, Meng X, Chen H, Thach TQ, Wong CM, Kan H (2013) Both low and high temperature may increase the risk of stroke mortality. Neurology 81(12):1064–1070. https://doi.org/10.1212/WNL.0b013e3182a4a43c

Christensen JH et al (2007) Regional climate projections. In: Solomon S et al (eds) Climate change 2007: the physical science basis. Contribution of Working Group I to the Fourth Assessment Report of the Intergovernmental Panel on Climate Change. Cambridge University Press, Cambridge, pp 847–940

Colette A, Vautard R, Vrac M (2012) Regional climate downscaling with prior statistical correction of the global climate forcing. Geophys Res Lett 39:L13707. https://doi.org/10.1029/2012GL052258

Collins W, Bellouin N, Doutriaux-Boucher M, Gedney N, Hinton T, Jones C, Liddicoat S, Martin G, O'Connor F, Rae J, Senior C, Totterdell I, Woodward S, Reichler T, Kim J (2008) Evaluation of the HadGEM2 model. Met Office Hadley Centre Technical Note no. HCTN 74, available from Met Office, FitzRoy Road, Exeter. http://www.metoffice.gov.uk/publications/HCTN/index.html. Accessed 15 Oct 2017

Environment Canada (2014) Canada's Wind Chill Index, Toronto, Canada, Catalogue No. En56-222/2-2008E, ISBN 978-0-662-47625-2

Fang S, Qi Y, Han G, Zhou G (2015) Changing trends and abrupt features of extreme temperature in mainland China during 1960 to 2010. Earth Syst Dyn Discuss 6:979–1000. https://doi.org/10.5194/esdd-6-979-2015

Feng J, Wang Y, Ma Z, Liu Y (2012) Simulating the regional impacts of urbanization and anthropogenic heat release on climate across China. J Clim 25(20):7187–7203. https://doi.org/10.1175/JCLI-D-11-00333.1

Flato G et al (2013) Evaluation of climate models. In: Stocker TF et al (eds) Climate change 2013: the physical science basis. Contribution of Working Group I to the Fifth Assessment Report of the Intergovernmental Panel on Climate Change. Cambridge University Press, Cambridge, pp 741–866

Frich P, Alexander LV, Della-Marta P, Gleason B, Haylock M, Klein AMG, Tank, Peterson T (2002) Observed coherent changes in climatic extremes during the second half of the twentieth century. Clim Res 19:193–212

Gao XJ, Wang M-L, Giorgi F (2013) Climate change over China in the 21st century as simulated by BCC_CSM1.1-RegCM4.0, Atmos. Ocean Sci Lett 6(5):381–386. https://doi.org/10.3878/j.issn.1674-2834.13.0029

Gong D, Yang J, Kim S, Gao Y, Guo D, Zhou T, Hu M (2011) Spring Arctic Oscillation-East Asian summer monsoon connection through circulation changes over the western North Pacific. Clim Dyn 37:2199–2216. https://doi.org/10.1007/s00382-011-1041-1

Harris I, Jones PD, Osborn TJ, Lister DH (2014) Updated high-resolution grids of monthly climatic observations—the CRU TS3.10 Dataset. Int J Climatol 34:623–642. https://doi.org/10.1002/joc.3711

Hartmann DL et al (2013) Observations: atmosphere and surface. In: Stocker TF et al (eds) Climate change 2013: the physical science basis. Contribution of Working Group I to the Fifth Assessment Report of the Intergovernmental Panel on Climate Change. Cambridge University Press, Cambridge, pp 159–254

Hewitson B, Janetos AC, Carter TR, Giorgi F, Jones RG, Kwon W-T, Mearns LO, Schipper ELF, van Aalst M (2014) Regional context, in climate change 2014: impacts, adaptation, and vulnerability. In: Barros VR et al (eds) Part B: regional aspects. Contribution of Working Group II to the Fifth Assessment Report of the Intergovernmental Panel on Climate Change. Cambridge University Press, Cambridge, pp 1133–1197

Jiang Y, Luo Y, Zhao Z, Shi Y, Xu Y, Zhu J (2010) Projections of wind changes for 21st century in China by three regional climate models. Chin Geogr Sci 20:226. https://doi.org/10.1007/s11769-010-0226-6

Jiang Y, Luo Y, Zhao Z (2013) Maximum wind speed changes over China. Acta Meteorol Sin 27:63. https://doi.org/10.1007/s13351-013-0107-x

Jiang L, Yan Y, Hararuk O, Mikle N, Xia J, Shi Z, Tjiputra J, Wu T, Luo Y (2015) Scale-dependent performance of CMIP5 earth system models in simulating terrestrial vegetation carbon. J Clim 28:5217–5232. https://doi.org/10.1175/JCLI-D-14-00270.1

Jones R, Noguer M, Hassell D, Hudson D, Wilson S, Jenkins G, Mitchell J (2004) Generating high resolution climate change scenarios using PRECIS. Met Office Hadley Centre, Exeter, p 40

Li H, Feng L, Zhou T (2011) Multi-model projection of July–August climate extreme changes over China under CO_2 doubling. Part II: temperature. Adv Atmos Sci 28:448. https://doi.org/10.1007/s00376-010-0052-x

Lin Z, Yu Z, Zhang H, Wu C (2016) Quantifying the attribution of model bias in simulating summer hot days in China with IAP AGCM 4.1. Atmospheric and Oceanic Sci Lett 9:6, 436–442, https://doi.org/10.1080/16742834.2016.1133071

Luo L, Tang W, Lin Z et al (2013) Evaluation of summer temperature and precipitation predictions from NCEP CFSv2 retrospective forecast over China. Clim Dyn 41:2213–2230. https://doi.org/10.1007/s00382-013-1927-1

Ma S, Zhou T, Stone D, Angelil O, Shiogama H (2017) Attribution of the July–August 2013 heat event in central and Eastern China to anthropogenic greenhouse gas emissions. Environ Res Lett 12:054020

MACA (2017) MACA Downscaling of CMIP5 GCMs, Multivariate Adaptive Constructed Analogs (MACA) Datasets. http://maca.northwestknowledge.net/GCMs.php. Accessed 15 Oct 2017

Martin GM, Bellouin N, Collins WJ et al (2011) The HadGEM2 family of met office unified model climate configurations. Geosci Model Dev 4(3):723–757. https://doi.org/10.5194/gmd-4-723-2011

Mearns, L.O., R.W. Katz, and S.H. Schneider (1984) Extreme high-temperature events: changes in their probabilities with changes in mean temperature. J Clim Appl Meteorol 23:1601–1613, https://doi.org/10.1175/1520-0450(1984)023%3C1601:EHTECI%3E2.0.CO;2.

Moss RH et al (2010) The next generation of scenarios for climate change research and assessment. Nature 463(7282):747–756. https://doi.org/10.1038/nature08823

Rupp DE, Abatzoglou JT, Hegewisch KC, Mote PW (2013) Evaluation of CMIP5 20th century climate simulations for the Pacific Northwest USA. J Geophys Res Atmos 118:10,884–10,906. https://doi.org/10.1002/jgrd.50843.

Song F, Zhou T (2014) Inter-annual variability of East Asian summer monsoon simulated by CMIP3 and CMIP5 AGCMs: skill dependence on Indian Ocean western Pacific anticyclone teleconnection. J Clim 27:1679–1697. https://doi.org/10.1175/JCLI-D-13-00248.1

Sperber KR, Annamalai H, Kang IS, Kitoh A, Moise A, Turner A, Wang B, Zhou T (2013) The Asian summer monsoon: an intercomparison of CMIP5 vs. CMIP3 simulations of the late 20th century. Clim Dyn 41(9–10):2711–2744. https://doi.org/10.1007/s00382-012-1607-6

Sun Q, Miao C, Duan Q (2015) Comparative analysis of CMIP3 and CMIP5 global climate models for simulating the daily mean, maximum, and minimum temperatures and daily precipitation over China. J Geophys Res Atmos 120:4806–4824. https://doi.org/10.1002/2014JD022994

Van Vuuren DP et al (2011) The representative concentration pathways: an overview. Clim Change 109:5–31. https://doi.org/10.1007/s10584-011-0148-z

Wang S, Huang GH (2015) A multi-level Taguchi-factorial two-stage stochastic programming approach for characterization of parameter uncertainties and their interactions: an application to water resources management. Eur J Oper Res 240:572–581. https://doi.org/10.1016/j.ejor.2014.07.011

Wang X, Huang G, Liu J (2014) Projected increases in near-surface air temperature over Ontario, Canada: a regional climate modeling approach. Clim Dyn. https://doi.org/10.1007/s00382-014-2387-y

Wang L, Li T, Zhou T (2015a) Effect of high-frequency wind on intraseasonal SST variabilities over the mid-latitude North Pacific region during boreal summer. Clim Dyn 45:2607–2617. https://doi.org/10.1007/s00382-015-2496-2

Wang S, Huang GH, Baetz BW, Huang W (2015b) A polynomial chaos ensemble hydrologic prediction system for efficient parameter inference and robust uncertainty assessment. J Hydrol 530:716–733. https://doi.org/10.1016/j.jhydrol.2015.10.021

Wang X, Huang G, Lin Q, Nie X, Liu J (2015c) High-resolution temperature and precipitation projections over Ontario, Canada: a coupled dynamical-statistical approach. QJR Meteorol Soc 141:1137–1146. https://doi.org/10.1002/qj.2421

Wang X, Li G, Liu L, Westerdahl D, Jin X, Pan X (2015Ddd) Effects of extreme temperatures on cause-specific cardiovascular mortality in China. Int J Environ Res Public Health 12(12):16136–16156. https://doi.org/10.3390/ijerph121215042

Wang S, Ancell BC, Huang GH, Baetz BW (2018) Improving robustness of hydrologic ensemble predictions through probabilistic pre- and post-processing in sequential data assimilation. Water Resour Res 54:2129–2151. https://doi.org/10.1002/2018WR022546

Wilson W, Hassell D, Hein D, Wang C, Tucker S, Jones R, Taylor R (2015) Technical manual for PRECIS: The Met Office Hadley Centre regional climate modelling system Version 2.0.0. http://www.metoffice.gov.uk/precis

Xu Y, Zhang Y, Lin E, Lin W, Dong W, Jones R, Hassell D, Wilson S (2006) Analyses on the climate change responses over China under SRES B2 scenario using PRECIS. Chin Sci Bull 51:2260–2267. https://doi.org/10.1007/s11434-006-2099-8

Xu J, Shi Y, Gao X, Giorgi F (2013) Projected changes in climate extremes over China in the 21st century from a high resolution regional climate model (RegCM3). Chin Sci Bull 58:1443. https://doi.org/10.1007/s11434-012-5548-6

Yao Y, Luo Y, Huang JB (2012) Evaluation and projection of temperature extremes over China based on CMIP5 model. Adv Clim Change Res 3(4):179–185. https://doi.org/10.3724/SP.J.1248.2012.00179

Yu E, Wang H, Sun J (2010) A quick report on a dynamical downscaling simulation over China using the nested model. Atmos Ocean Sci Lett 3(6):325–329. https://doi.org/10.1080/16742834.2010.11446886

Zhai P, Pan X (2003) Trends in temperature extremes during 1951–1999 in China. Geophys Res Lett 30(17):1913. https://doi.org/10.1029/2003GL018004

Zhang H, Fraedrich K, Blender R, Zhu X (2013) Precipitation extremes in CMIP5 simulations on different time scales. J Hydrometeorol 14:923–928. https://doi.org/10.1175/JHM-D-12-0181.1

Zhou T, Song F, Chen X (2013) Historical evolutions of global and regional surface air temperature simulated by FGOALS-s2 and FGOALS-g2: how reliable are the model results? Adv Atmos Sci 30(3):638–657. https://doi.org/10.1007/s00376-013-2205-1